Polymer Chemistry

ROYAL SOCIETY OF CHEMISTRY

PAPER

View Article Online
View Journal | View Issue

Cite this: *Polym. Chem.*, 2020, **11**, 4040

Discrete multifunctional sequence-defined oligomers with controlled chirality†

Jie Li,[a] Maxime Leclercq,[b] Mathieu Fossepré,[b] Mathieu Surin,*[b] Karine Glinel,[a] Alain M. Jonas*[a] and Antony E. Fernandes*[a,c]

Received 13th April 2020,
Accepted 28th May 2020

DOI: 10.1039/d0py00537a

rsc.li/polymers

Discrete sequence-defined oligomers are synthetic mimics of short peptides, with possible applications in catalysis, information storage, drug delivery or self-assembly. Here, we report on the efficient and stereocontrolled synthesis of sequence-defined poly(triazole-urethane) oligomers incorporating a very large range of functional side groups, including alkyl, phenyl, pyridyl, hydroxyl, amine, imidazole and carboxylic acid functions. The route involves the alternation of chloroformate-mediated carbamate bond formation and Cu-catalyzed azide–alkyne cycloaddition reactions, expeditiously leading to oligomers up to octamers by an iterative exponential growth strategy. Additionally, the chirality of the monomers is straightforwardly controlled and maintained during the elongation process, leading to optically-active multifunctional oligomers of controlled molecular configuration, as confirmed by ^{1}H NMR, ESI-MS/MS and circular dichroism. Our strategy provides a versatile platform to efficiently synthesize discrete oligomers with programmable stereochemistry, sequentiality and multifunctionality.

Introduction

Sequence and stereoregularity are central to the functioning of biomacromolecules such as proteins or nucleic acids. Reaching a similar degree of control over primary structure and chirality in synthetic polymers has been a long endeavor,[1] including the catalytic control of tacticity,[2,3] the development of reversible deactivation routes for the control of molar mass,[4–7] and the more recent emergence of synthetic strategies towards sequence-defined polymers.[8–19] For that latter purpose, iterative stepwise methods, including iterative sequential growth (ISG) and iterative exponential growth (IEG), have generally been developed.[20–24] In particular, IEG strategies provide rapid access to longer precision oligomers as the chain length is doubled after each iterative cycle, even though they are restricted to the production of symmetric products in which not every repeat unit is freely selectable. Hence, monomers bearing orthogonal protective groups, or latent functional groups,[17,25,26] are activated divergently, releasing complementary-activated units, to be convergently reunified. It is however possible to go beyond the repetitive or palindromic primary structures typically obtained by IEG. For instance, the IEG+ strategy developed by Johnson and coll. combines both exponential chain growth and side chain functionalization.[15,27,28]

Although such routes are effective in terms of sequence control, they rarely achieve a simultaneous control over stereochemistry, and most often have a limited tolerance towards the more reactive functional side groups typically found in natural polymers, responsible for catalytic activity for instance. Since one of the possible fields of application of discrete sequence-defined polymers is precisely multifunctional or cascade catalysis, as we demonstrated recently by showing that sequence order controls the catalytic activity of trifunctional catalytic oligomers,[29,30] it becomes critical to develop more tolerant routes leading to chains of controlled sequence. Additionally, controlled stereochemistry, as typically present in enzymes, is also a very desirable feature for catalysis with the aim to further control the tridimensional arrangement of cooperative catalytic sites.

Here, we concentrate on the development of a synthetic route to reach this goal, and propose an innovative strategy leading to precision oligomers of controlled sequence and stereochemistry capable to incorporate a wide range of functional groups – such as those found in proteins – based on the copper-catalyzed azide–alkyne cycloaddition (CuAAC) "click" reaction.[31] The CuAAC reaction, due to its high efficiency and chemoselectivity, was previously demonstrated to be a promising tool for the synthesis of sequence-defined

[a]*Institute of Condensed Matter and Nanosciences, Bio- and Soft Matter, Université catholique de Louvain, 1348 Louvain-la-Neuve, Belgium*
[b]*Laboratory for Chemistry of Novel Materials, Centre of Innovation and Research in Materials and Polymers (CIRMAP), University of Mons - UMONS, 20 Place du Parc, 7000 Mons, Belgium. E-mail: mathieu.surin@umons.ac.be*
[c]*Certech, Rue Jules Bordet 7180 Seneffe, Belgium*

†Electronic supplementary information (ESI) available. See DOI: 10.1039/d0py00537a

polymers.[12,23,25,27,32–35] This archetypal "click" reaction was for instance successfully used to obtain sequence-defined and stereocontrolled polymers, yet mainly limited to side groups of lesser reactivity.[15,27,28,33] Building onto these previous works, we demonstrate a new strategy leading to discrete stereocontrolled and sequence-defined oligomers capable of accommodating a wide range of functional side groups alike natural peptides, albeit at a lower chain density.

Experimental

Experimental and simulation details are given in the ESI.†

Results and discussion

The main building blocks were prepared starting from TBDMS-protected glycidyl propargyl ether **1** either in its racemic (*rac*-**1**) or enantiopure ((*R*)-**1** or (*S*)-**1**) forms (TBDMS = *tert*-butyldimethylsilyl) (Scheme 1a).[27] To prove the validity of our concept, the strategy was first developed starting from racemic *rac*-**1**. Side groups were inserted following opening of the oxirane ring of *rac*-**1** with sodium azide and subsequent CuAAC reaction of **2** with alkynes **3a–d** to provide functional monomers **4a–d** with overall yields varying between 87% and quantitative. Noteworthy, alkynes **3a–d** bearing respectively phenyl, pyridyl, methoxy and *t*-butyl groups were carefully selected to provide unique, unambiguous ^{1}H NMR footprints in order to trace the composition of the oligomers.

From this, key to our strategy is the efficient re-introduction of the azide group and release of the free alkyne to enable chain elongation through CuAAC reaction. In this purpose, the secondary alcohol of building blocks **4a** and **4b** was first treated with *p*-nitrophenyl chloroformate (PNPCF) to yield the activated carbonate intermediate that was directly reacted with 3-azidopropylamine. This one pot procedure provides nearly quantitative yields of the monomers **5a** and **5b** bearing a stable carbamate bond within the main chain (92 and 87% yield, respectively).

Compared to previous work based on similar chemistry,[15,27,28] our approach essentially differs by exchan-

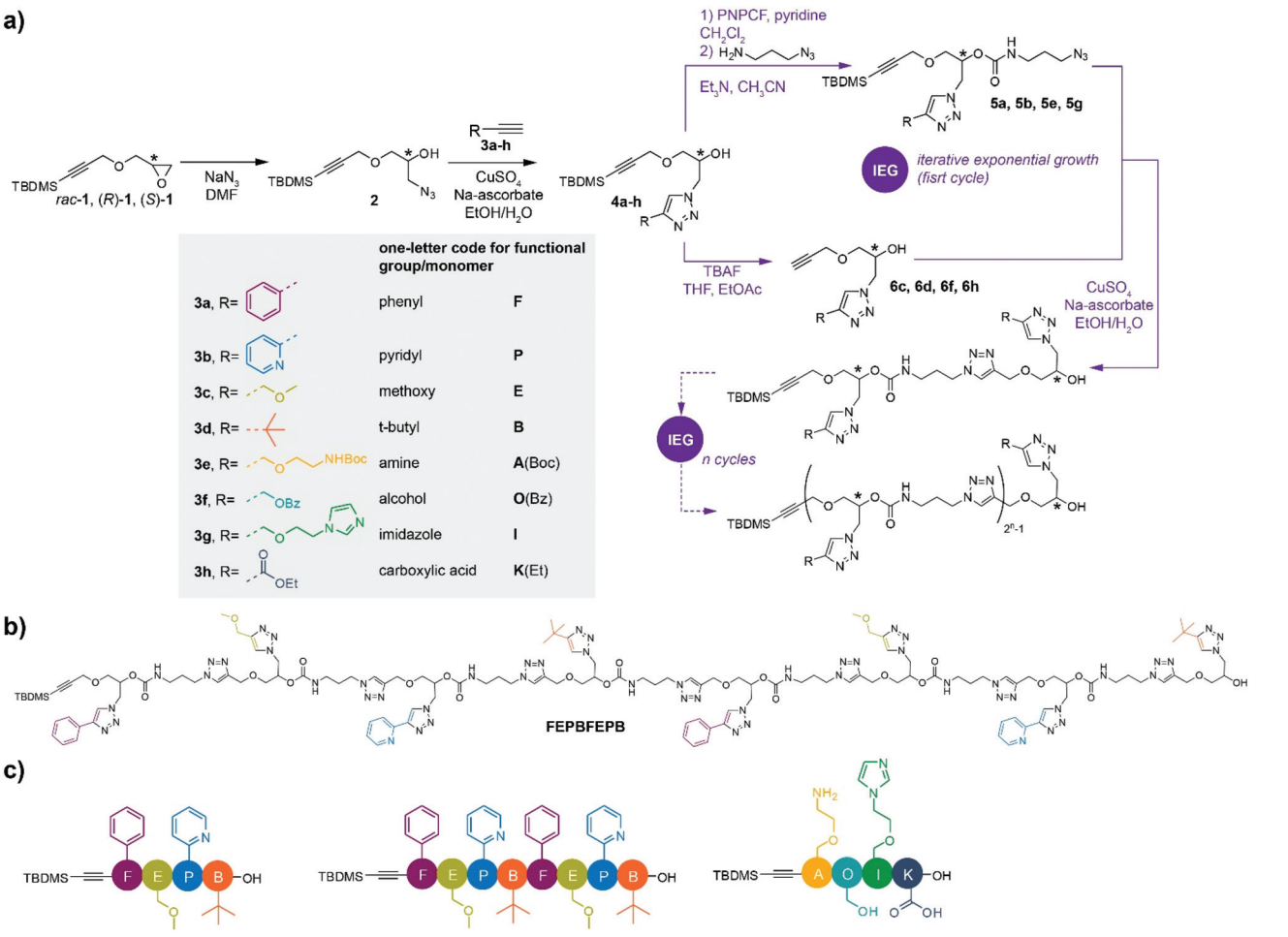

Scheme 1 . Iterative exponential growth (IEG) strategy to generate discrete multifunctional stereocontrolled sequence-defined oligomers. (a) Synthetic scheme and one-letter code. (b) Structure of octamer **FEPBFEPB** obtained after 3 IEG cycles. (c) Simplified illustration of the obtained oligomers **FEPB**, **FEPBFEPB** and **AOIK**.

ging the functionalities used for installing the side chain groups and extending the chain backbone, which is a minor modification; and, much more crucially, by replacing ester groups by the considerably more stable carbamate groups, which is required for the installation of a much wider range of functional groups on the chains than could be done before. Indeed, we have recently shown that ester groups are not suitable in such a scheme, being not stable enough under hydrolytic and TBAF (tetrabutylammonium fluoride) conditions.[29,36]

Meanwhile, removal of the TBDMS group in **4c** and **4d** using TBAF provided free alkynes **6c** and **6d** (71 and 90% yield, respectively). Coupling of the obtained azides and alkynes yielded the dimeric species that allowed pursuing an IEG strategy towards higher oligomers. For clarity, a simple one-letter code was adopted for the naming of the different functional side groups/monomers that is inspired from the nomenclature used for natural amino acids (Scheme 1a).[37] For instance, reaction of **5a** with **6c** under CuAAC conditions gives dimer **FE** (93% yield) bearing a phenyl (F) and a methoxy (E) side group, while reaction of **5b** with **6d** bearing a pyridyl (P) and *tert*-butyl (B) side group, respectively, afforded dimer **PB** (80% yield). A subsequent IEG cycle provided tetramer **FEPB** (72% yield); the later allowing access to octamer **FEPBFEPB** (Scheme 1b) in 57% yield through another IEG cycle. The overall yield of the octamer, starting from the protected monomers **4a–d**, was 27%, providing access to milligrams of chains in our conditions. Of note, we did not face solubility issues for our oligomers despite their high content in triazole groups, possibly due to the functional similarity of such groups with amides.[38]

The stacked ^{1}H NMR spectra of monomers **4a–d** show that the signals corresponding to the pendant phenyl, pyridine, methoxy and *tert*-butyl protons do not overlap, as anticipated (Fig. 1a–d). Additionally, the triazole proton experiences different chemical environments in monomers **4a–d**, which translates into different chemical shifts; this provides an additional way to identify the monomer units after their insertion in the oligomers. Precisely, the ^{1}H NMR spectra of tetramer **FEPB** and octamer **FEPBFEPB** evidence the presence of the expected characteristic peaks of each monomeric unit together with the additional resonances corresponding to the parent azidopropylamine moiety in the main chain (Fig. 1e and f).

In addition to ^{1}H NMR analysis, electrospray ionization mass spectrometry (ESI-MS) confirmed the structure of the monomers and oligomers (ESI†). For instance, ESI-MS of the octamer **FEPBFEPB** displayed peaks at m/z = 2952.5932, 1476.8147, 984.8832, 738.9161 and 591.3353 corresponding to the theoretical values for $[M + H]^+$, $[M + 2H]^{2+}$, $[M + 3H]^{3+}$, $[M + 4H]^{4+}$ and $[M + 5H]^{5+}$, respectively (Fig. S128†) The molecular sequence of the oligomers was deciphered using tandem mass spectrometry (ESI-MS/MS).

Cleavage of the ether bond in the main chain, yielding to two series of complementary fragments, was detected as the most prominent fragmentation mechanism in tetramer **FEPB** (Fig. S134†) and octamer **FEPBFEPB** (Fig. 2). According to this

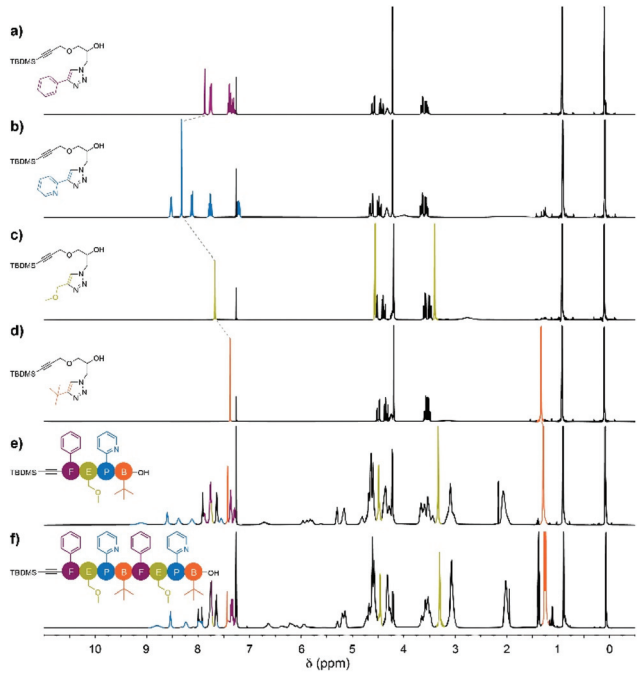

Fig. 1 Stacked ^{1}H NMR (300 MHz, $CDCl_3$) of (a) **4a**, (b) **4b**, (c) **4c** and (d) **4d**; the dashed line connects resonances of the triazole proton within the different monomers. Stacked ^{1}H NMR (500 MHz, $CDCl_3$) of (e) tetramer **FEPB** and (f) octamer **FEPBFEPB**.

mechanism, the sequence of **FEPBFEPB** reading from left to right were recorded with m/z = 536.32, 887.50, 1271.70, 1634.91, 2018.06, 2369.11 and 2753.04 corresponding respectively to the sequence **F**, **FE**, **FEP**, **FEPB**, **FEPBF**, **FEPBFE** and **FEPBFEP**. Additionally, reading the sequence from the right side displayed a peak at m/z = 182.14 corresponding to monomer **B**. Thus, the sequence in the octamer **FEPBFEPB** was unraveled by ESI-MS/MS, which was confirmed from the right to left side as well. Overall, the fragmentation patterns unambiguously confirm that all the synthesized oligomers have the desired sequence.

In order to further illustrate the versatility of our strategy, oligomers comprising a wider variety of functional side groups were synthesized. Thus, inspired by functional side groups found in natural amino acids, monomers comprising pendant amine (A), hydroxyl (O), imidazole (I) and carboxylic acid (K) side groups were synthesized (Scheme 1). Owing to the very chemistry involved in our approach, it was necessary to protect the nucleophilic side groups in order not to interfere with the elongation steps. Hence, A, O and K were protected with *tert*-butoxycarbonyl (Boc), benzoyl (Bz) and ethyl (Et) groups, respectively. Following the IEG procedure described above, tetramer **A(Boc)O(Bz)IK(Et)** was obtained in 35% overall yield after two IEG cycles. Final treatment of **A(Boc)O(Bz)IK(Et)** with trifluoroacetic acid and KOH provided the targeted **AOIK** tetramer in quantitative yield without hydrolysis of the main chain.

The structure of **AOIK** and its protected precursor **A(Boc)O(Bz)IK(Et)** was confirmed by ^{1}H NMR (Fig. S99–S101†) and ESI-MS (Fig. S129–S130†). As previously, the sequence

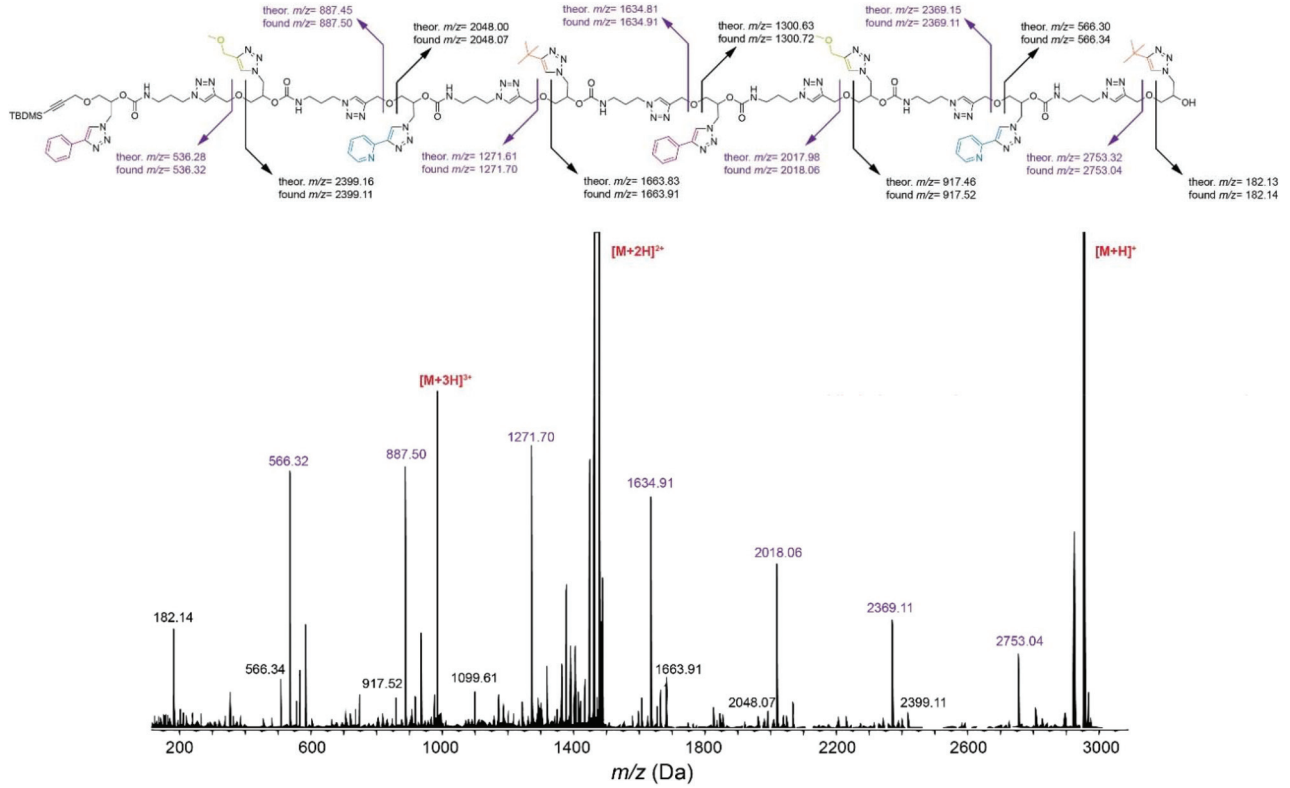

Fig. 2 ESI-MS/MS sequencing of octamer **FEPBFEPB** obtained after collisional activation of the $[M + H]^+$ precursor at m/z = 2952 Da.

information was confirmed by tandem mass spectrometry (Fig. S139† for **AOIK**, and S138 for its protected version). Interestingly, the negative mode ESI-MS/MS was successfully developed to trace the sequence from the right to the left side of **AOIK** owing to the contribution of carboxylic acid group in the side chain (Fig. S140†). Especially, preservation of the integrity of the oligomers (composition and sequence) after complete cleavage of the protecting groups was confirmed, demonstrating the tolerance of our synthetic strategy to a wide variety of chemistries and functional groups.

Although synthetic methods are flourishing to access sequence-defined oligomers, a very limited number of synthetic strategies have been reported to control both sequence and chirality,[15,27,28,39] a situation that is ever more challenging when multiple functional groups are involved within the chain. Therefore, a set of enantiopure monomers bearing F, E, P and B side groups was synthesized starting from chiral TBDMS-protected glycidyl propargyl ether (*R*)-**1** or (*S*)-**1**[27] (Scheme 1a). The enantiomeric excess (ee) of the monomers was traced by chiral HPLC, in which **4a** was carried out as the example (Fig. S141†). The ee of (*R*)-**4a** and (*S*)-**4a** were 90 and 88%, respectively, showing that the chirality was well controlled under the synthetic processes. Stereocontrolled sequence-defined oligomers (*R*,*R*,*R*,*R*)-**FEPB**, (*S*,*S*,*S*,*S*)-**FEPB** and (*R*,*R*,*R*,*R*,*S*,*S*,*S*,*S*)-**FEPBFEPB** were straightforwardly prepared employing the IEG strategy developed for *rac*-**1** (Scheme 1a). As expected, their ^{1}H NMR, ESI-MS and ESI-MS/MS spectra were identical to the ones of the racemic oligomers (ESI†). The maximum content of the (*R*,*R*,*R*,*R*,*S*,*S*,*S*,*S*)-**FEPBFEPB** octamer in oligomers of lower length was estimated from the ratio of ^{1}H NMR peaks between 0.86 and 0.96 ppm (*t*-butyl silyl-) and 5.00–5.34 ppm (protons of the asymmetric carbons of all monomer units except the terminal one); it was found to be at most 5% by number, and very likely much lower. HPLC confirmed the very high purity of the stereocontrolled tetramers and octamer (Fig. S149–S151†).

Circular dichroism (CD) spectroscopy provided qualitative information on the stereochemistry of the chains. The CD spectra of monomers **4a–d** and dimers **FE** and **PB** (Fig. S142†) with (*R*)- and (*S*)-configurations show opposite signals as expected for enantiomers. Likewise, the CD spectra of dilute solutions of the tetramers (*R*,*R*,*R*,*R*)-**FEPB** and (*S*,*S*,*S*,*S*)-**FEPB** show opposite signals peaking at 212 nm (Fig. 3a and Fig. S143†), confirming that the two tetramers have mirror configurations. In contrast, octamer (*R*,*R*,*R*,*R*,*S*,*S*,*S*,*S*)-**FEPBFEPB** exhibits a significantly weaker CD signal (Fig. 3a) because it contains identical amounts of tetrameric (*S*) and (*R*) sequences; the non-suppression of the CD signal results from the fact that the octamer nevertheless lacks centers and planes of symmetry. Overall, the CD results thus clearly indicate that the stereochemistry is utterly controlled, and racemization does not occur during the IEG process. Of note, since the enantiomeric excess of our starting monomer units is currently *ca.* 90% only, our oligomers are still mixtures of a series of

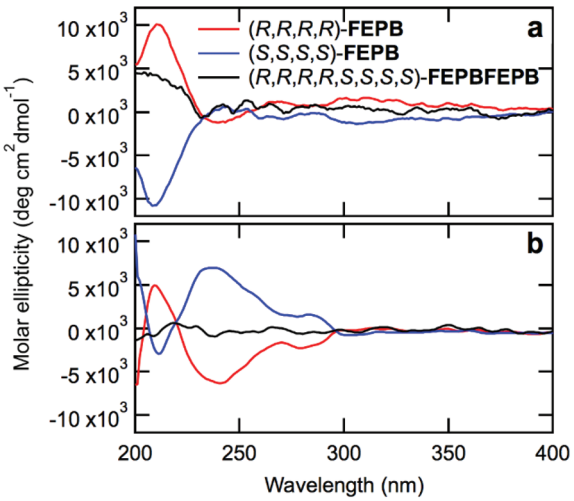

Fig. 3 Circular dichroism spectra of (*R*,*R*,*R*,*R*)-**FEPB** (red), (*S*,*S*,*S*,*S*)-**FEPB** (blue) and (*R*,*R*,*R*,*R*,*S*,*S*,*S*,*S*)-**FEPBFEPB** (black) in CH_3CN. Concentrations are (a) 30 μM and 15 μM for the tetramers and octamer, respectively; (b) 150 μM and 75 μM for the tetramers and octamer, respectively. The spectra were smoothed (Savitzky–Golay, 13-point, second order polynomial).

stereochemical configurations, which does not prevent them from displaying a strong circular dichroism. An even narrower distribution of stereochemical configuration could be obtained by starting from a more enantiopure form of **2**, as discussed elsewhere.[14]

Interestingly, at a five times higher concentration (Fig. 3b and Fig. S144†), the CD spectra of (*R*,*R*,*R*,*R*)- and (*S*,*S*,*S*,*S*)-**FEPB** display additional mirror peaks at 238 and 283 nm, which is likely due to aggregation of the chains and suggests that the aggregated states of the oligomers remain chiral. As before, the (*R*,*R*,*R*,*R*,*S*,*S*,*S*,*S*)-**FEPBFEPB** octamer only exhibits a weak signal. To further understand the aggregation behavior of the oligomers, all-atom Molecular Dynamics (MD) simulations were carried out from the single chain level to assemblies of a few chains (see ESI† for computational details). MD simulations of a single chain provided structural and dynamical aspects of the octamer (*R*,*R*,*R*,*R*,*S*,*S*,*S*,*S*)-**FEPBFEPB.**

The octamer rapidly folds into a compact globular structure (Fig. 4a), characterized by a low radius of gyration (R_g) of 7.4 Å in average, very low compared to the end-to-end distance of the fully elongated conformation (around 100 Å, see ESI S145†). The stability of R_g profile over time (ESI S146†) indicates that the globular folding is preserved on the microsecond timescale. Although a total of 93 hydrogen bonds were detected for all conformations of the MD, most of them are not persistent: 88 H-bonds are present for less than 10% of the MD time, and none was detected for more than 50% of the MD time (see ESI S147†). This large number of possible H-bonds arises from each repeat unit containing one carbamate group, plus two triazole groups which are good mimetics of secondary amide groups with respect to H-bonding donor/acceptor capabilities.[38,40] The network of H-bonds is constantly evolving and important oscillations in the number of H-bonds are observed throughout MD time (Fig. 4b), varying from 0 to 7 H-bonds with an average of only 2–3 H-bonds per conformation. Therefore, H-bonds are only weakly participating to the compact globular folding of the octamer. In contrast, the numerous aromatic moieties located on the side chains and along the backbone, labeled on top of Fig. 4, provide many possibilities of π-stacking interactions. The distances between the centers-of-mass (COM) of all depicted aromatic pairs were estimated. As for H-bonds, the network of aromatic interactions is dynamic and a criterion (at least 50% of MD time at a distance below 5.0 Å) was considered to point out the most persistent aromatic interactions. Some of these most persistent stacking interactions are depicted on the final MD snapshot in Fig. 4c and d. With this criterion, six π-stacking interactions are persistent: one is involving two triazole moieties of the backbone (labelled as **13** and **15** in Fig. 4), two interactions concern backbone/side-chain aromatic moieties (**5a–12** and **5b–14** pairs) and three interactions are occurring between side-chains (**5a–8**, **3a–6**, and **3b–6**). These persistent π-stacking interactions between aromatic groups far in the octamer sequence but close in space evidently contribute to stabilize the compact globular conformations of the oligomer.

MD simulations involving either two chains or five chains were performed to investigate the driving force and dynamics for the aggregation of the octamer. For both MD simulations, octamer chains rapidly form a supramolecular complex that remains stable on the microsecond time scale, *i.e.* no dissociation between the chains were observed. Interestingly, self-assemblies of 2 chains or 5 chains do not show any intertwining between the chains (see MD snapshots in Fig. 4e and f). In comparison to the MD simulations of a single chain, only a minor increase of the average R_g is observed in the assembly of two chains (ESI S146†). The compactness of both chains in the assembly is similar as the average R_g of both chains converge to identical values. In the assembly of 5 chains, compact conformations are again observed, but with a slightly higher average R_g (around 10 Å). Concerning the dynamics of the octamer, the flexibility profile along the chain of the octamer (as estimated with Root-Mean-Square Fluctuations estimates, see ESI S148†) differs for the single chain and for the assemblies. Importantly, the flexibility of a single octamer chain can be discriminated inside the aggregate. For example, the octamer #1 corresponding to the chain colored in black in Fig. 4f is more rigid than the other octamers, because of its more compact folding (lower average R_g). Altogether, our results show that (*R*,*R*,*R*,*R*,*S*,*S*,*S*,*S*)-**FEPBFEPB** octamers fold into very compact structures, mainly stabilized by persistent π-stacking interactions, whereas hydrogen bonds are not persistent. Given the numerous possibilities of stacking interactions, stable assemblies of several chains are observed in which structural aspects and the dynamics of octamers can be influenced by the number of chains within the assembly. Altogether, this indicates that the oligomers studied in this work are prone to compact folding and assembly into

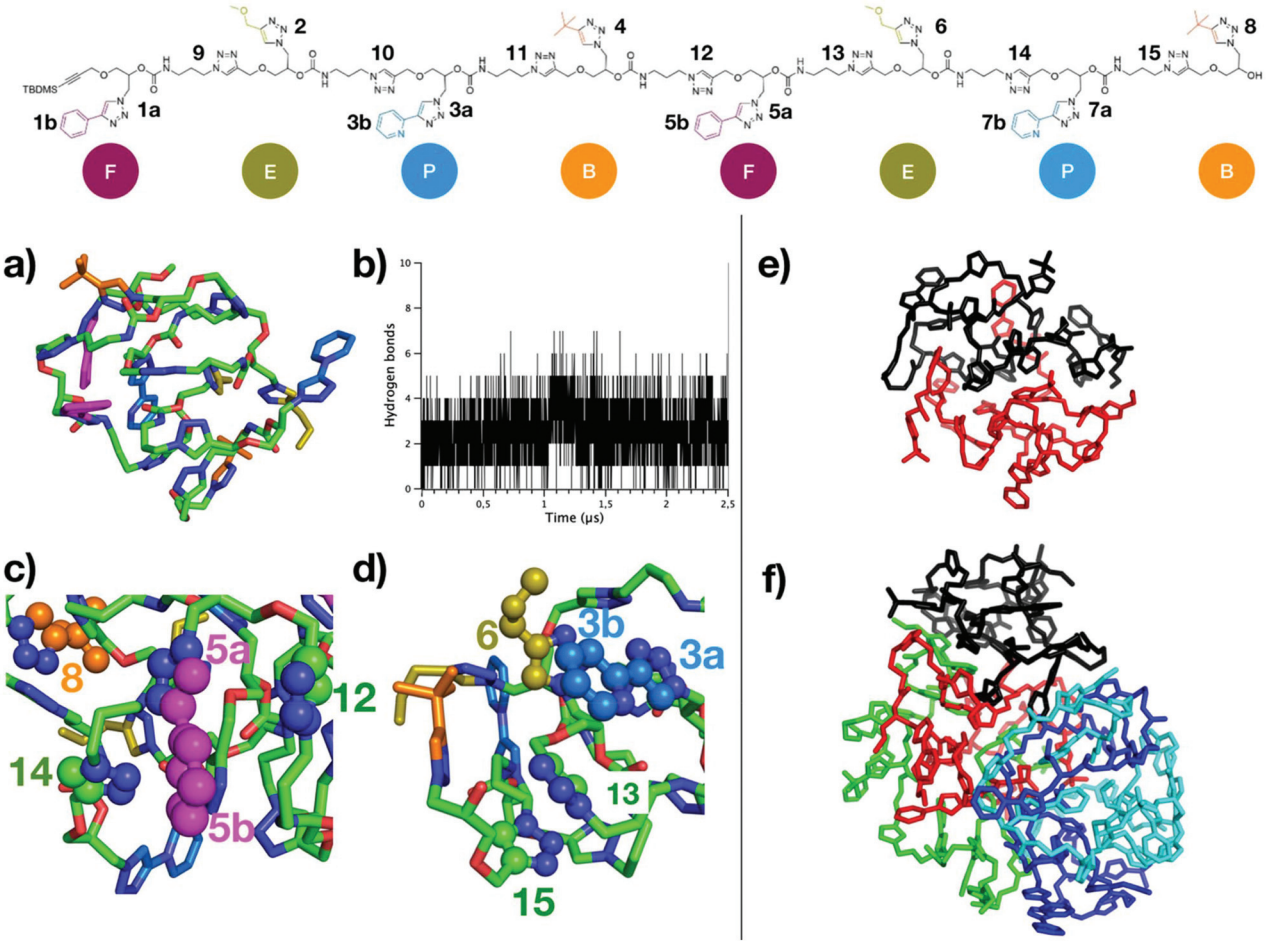

Fig. 4 (a) Final MD snapshot representative of the folded conformation of (*R*,*R*,*R*,*R*,*S*,*S*,*S*,*S*)-**FEPBFEPB** octamer. (b) Number of hydrogen bonds along MD time. (c) Proximity of specific aromatic moieties (in spheres) that are involved in some of the most persistent π-stacking interactions (numbering refer to the labels shown on the top chemical structure). Aromatic groups labelled as **5a** interact with **12**, and **5b** interacts with **14**. (d) Both **3a** and **3b** interact with **6**, and **13** interacts with **15**. (e–f) Final MD snapshots of assemblies of 2 chains and 5 chains are depicted in (e) and (f), respectively. Each octamer is shown in a one color and only heavy atoms are represented for the sake of clarity.

quaternary structures because of the numerous π-stacking interactions.

Conclusions

In conclusion, we report on a straightforward and efficient approach for the synthesis of discrete multifunctional stereocontrolled sequence-defined oligomers. The method provides rapid access to optically-active poly(triazole-urethane) oligomers bearing triazole-linked side chains, with a broad range of possible functional side groups reminiscent of those found in proteins, albeit at a smaller linear density. Another difference is that the folding and aggregation of oligomers is most likely driven by π-stacking interactions, as revealed by MD simulations, whereas the numerous possible H-bonding interactions play a much more minor role. These oligomers offer attractive perspectives for multifunctional catalysis and self-assembly, applications for which octameric sequences are more than long enough as we demonstrated previously.[29]

Conflicts of interest

There are no conflicts to declare.

Acknowledgements

The authors acknowledge the Fonds de la Recherche Scientifique - FNRS and the Fonds Wetenschappelijk Onderzoek under EOS project no. 30650939 for financial support. A.E.F. acknowledges the European Regional Development Fund (ERDF) and Wallonia Operational Program "Wallonia-2020.EU". M.L. and M.S. acknowledge the Wallonia Region and FNRS under grant no. F.4532.16. The authors acknowledge Gabriella Barrozino-Consiglio for 500 MHz NMR analysis, Raoul Rozenberg for APCI-MS, Hervé Degand for ESI-MS/MS analysis and Laurent Collard for HPLC analysis. Computational resources have been provided by the Consortium des équipements de Calcul Intensif (CéCI), funded by the FNRS under grant 2.5020.11.

KG and MS are Senior Research Associates of the F. R. S.–FNRS.

References

1 J.-F. Lutz, J.-M. Lehn, E. W. Meijer and K. Matyjaszewski, *Nat. Rev. Mater.*, 2016, **1**, 1–14.
2 G. W. Coates, *Chem. Rev.*, 2000, **100**, 1223–1252.
3 L. E. Rosebrugh, V. M. Marx, B. K. Keitz and R. H. Grubbs, *J. Am. Chem. Soc.*, 2013, **135**, 10032–10035.
4 K. Satoh and M. Kamigaito, *Chem. Rev.*, 2009, **109**, 5120–5156.
5 A. S. Barrow, C. J. Smedley, Q. Zheng, S. Li, J. Dong and J. E. Moses, *Chem. Soc. Rev.*, 2019, **48**, 4731–4758.
6 J. Yeow, R. Chapman, A. J. Gormley and C. Boyer, *Chem. Soc. Rev.*, 2018, **47**, 4357–4387.
7 N. Badi and J. F. Lutz, *Chem. Soc. Rev.*, 2009, **38**, 3383–3390.
8 E. Maron, J. H. Swisher, J. Haven, T. Y. Meyer, T. Junkers and H. G. Börner, *Angew. Chem., Int. Ed.*, 2019, **58**, 10747–10751.
9 W. Konrad, C. Fengler, S. Putwa and C. Barner-Kowollik, *Angew. Chem., Int. Ed.*, 2019, **58**, 7133–7137.
10 R. Dong, R. Liu, P. R. J. Gaffney, M. Schaepertoens, P. Marchetti, C. M. Williams, R. Chen and A. G. Livingston, *Nat. Chem.*, 2019, **11**, 136–145.
11 S. Celasun, D. Remmler, T. Schwaar, M. G. Weller, F. Du Prez and H. G. Borner, *Angew. Chem., Int. Ed.*, 2019, **58**, 1960–1964.
12 C. Yang, J. P. Flynn and J. Niu, *Angew. Chem., Int. Ed.*, 2018, **57**, 16194–16199.
13 S. Martens, A. Landuyt, P. Espeel, B. Devreese, P. Dawyndt and F. Du Prez, *Nat. Commun.*, 2018, **9**, 4451.
14 Z. Huang, B. B. Noble, N. Corrigan, Y. Chu, K. Satoh, D. S. Thomas, C. J. Hawker, G. Moad, M. Kamigaito, M. L. Coote, C. Boyer and J. Xu, *J. Am. Chem. Soc.*, 2018, **140**, 13392–13406.
15 M. R. Golder, Y. Jiang, P. E. Teichen, H. V. Nguyen, W. Wang, N. Milos, S. A. Freedman, A. P. Willard and J. A. Johnson, *J. Am. Chem. Soc.*, 2018, **140**, 1596–1599.
16 J. Xu, C. Fu, S. Shanmugam, C. J. Hawker, G. Moad and C. Boyer, *Angew. Chem., Int. Ed.*, 2017, **56**, 8376–8383.
17 M. Porel, D. N. Thornlow, N. N. Phan and C. A. Alabi, *Nat. Chem.*, 2016, **8**, 590–596.
18 S. Wang, Y. Tao, J. Wang, Y. Tao and X. Wang, *Chem. Sci.*, 2019, **10**, 1531–1538.
19 J. De Neve, J. J. Haven, L. Maes and T. Junkers, *Polym. Chem.*, 2018, **9**, 4692–4705.
20 R. B. Merrifield, *J. Am. Chem. Soc.*, 1963, **85**, 2149–2154.
21 O. I. Paynter, D. J. Simmonds and M. C. Whiting, *J. Chem. Soc., Chem. Commun.*, 1982, **20**, 1165–1166.
22 F. A. Leibfarth, J. A. Johnson and T. F. Jamison, *Proc. Natl. Acad. Sci. U. S. A.*, 2015, **112**, 10617–10622.
23 F. Amir, Z. Jia and M. J. Monteiro, *J. Am. Chem. Soc.*, 2016, **138**, 16600–16603.
24 S. C. Solleder, R. V. Schneider, K. S. Wetzel, A. C. Boukis and M. A. R. Meier, *Macromol. Rapid Commun.*, 2017, **38**, 1600711.
25 J. Niu, R. Hili and D. R. Liu, *Nat. Chem.*, 2013, **5**, 282–292.
26 S. Martens, J. Van den Begin, A. Madder, F. E. Du Prez and P. Espeel, *J. Am. Chem. Soc.*, 2016, **138**, 14182–14185.
27 J. C. Barnes, D. J. Ehrlich, A. X. Gao, F. A. Leibfarth, Y. Jiang, E. Zhou, T. F. Jamison and J. A. Johnson, *Nat. Chem.*, 2015, **7**, 810–815.
28 Y. Jiang, M. R. Golder, H. V. Nguyen, Y. Wang, M. Zhong, J. C. Barnes, D. J. Ehrlich and J. A. Johnson, *J. Am. Chem. Soc.*, 2016, **138**, 9369–9372.
29 P. Chandra, A. M. Jonas and A. E. Fernandes, *J. Am. Chem. Soc.*, 2018, **140**, 5179–5184.
30 P. Chandra, A. M. Jonas and A. E. Fernandes, *ACS Catal.*, 2018, **8**, 6006–6011.
31 V. V. Rostovtsev, L. G. Green, V. V. Fokin and K. B. Sharpless, *Angew. Chem., Int. Ed.*, 2002, **41**, 2596–2599.
32 M. Ciaccia, D. Nunez-Villanueva and C. A. Hunter, *J. Am. Chem. Soc.*, 2019, **141**, 10862–10875.
33 N. F. Konig, A. Al Ouahabi, S. Poyer, L. Charles and J. F. Lutz, *Angew. Chem., Int. Ed.*, 2017, **56**, 7297–7301.
34 D. Núñez-Villanueva, M. Ciaccia, G. Iadevaia, E. Sanna and C. A. Hunter, *Chem. Sci.*, 2019, **10**, 5258–5266.
35 R. Szweda, C. Chendo, L. Charles, P. N. W. Baxter and J.-F. Lutz, *Chem. Commun.*, 2017, **53**, 8312–8315.
36 P. Chandra, A. M. Jonas and A. E. Fernandes, *RSC Adv.*, 2019, **9**, 14194–14197.
37 M. Saffran, *Biochem. Educ.*, 1998, **26**, 116–118.
38 Y. L. Angell and K. Burgess, *Chem. Soc. Rev.*, 2007, **36**, 1674–1689.
39 N. Franz, L. Menin and H.-A. Klok, *Eur. J. Org. Chem.*, 2009, **2009**, 5390–5405.
40 M. Corredor, J. Solà and I. Alfonso, in *Targets in Heterocyclic Systems*, 2017, vol. 21, ch. 1, pp. 1–22.

